THE JOURNAL OF PHYSICAL CHEMISTRY C
A JOURNAL OF THE AMERICAN CHEMICAL SOCIETY

pubs.acs.org/JPCC

Article

Symmetry-Breaking Charge Separation and Null Aggregates

Frank C. Spano*

Cite This: J. Phys. Chem. C 2024, 128, 248−260

Read Online

ACCESS | Metrics & More | Article Recommendations

ABSTRACT: The relationship between symmetry-breaking charge separation (SB-CS) and null aggregate (NA) formation in molecular dimer complexes is investigated theoretically, with applications mainly to dimers based on PDI chromophores. Both processes derive from null points, which are defined by degeneracies in either the upper or lower adiabatic exciton bands. The Hamiltonian contains intermolecular coupling derived from the interacting molecular transition dipole moments (Coulomb coupling), which gives rise to Frenkel excitons, as well as the coupling between the Frenkel excitons and charge-transfer (CT) excitons, driven by the electron (t_e) and hole (t_h) hopping integrals. A recipe for efficient SB-CS is presented, which, beyond the Weller condition—which holds that the solvent-stabilized CT state should appear below the optical gap -includes two additional conditions: the presence of a null point and, just as important, lopsided electron and hole transfer integrals, $|t_e| \gg |t_h|$ or $|t_h| \gg |t_e|$. When such conditions are met, the developing charge asymmetry is optimized in response to small fluctuations in the polar solvent-induced electric field, which eventually leads to the solvent-stabilized charge-separated state. It is shown that SB-CS can also occur in H-dimers with significant cofacial overlap, consistent with the observations made by several groups.

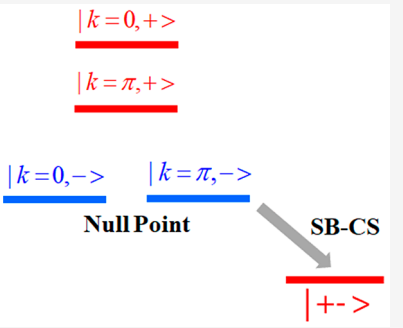

I. INTRODUCTION

Symmetry-breaking charge separation (SB-CS) is an important photophysical process in which an optically excited molecular system with an initially symmetric charge distribution rapidly relaxes into an asymmetrically charge-separated state. SB-CS has received a great deal of attention for its central role in photosynthesis, where the charge separation event within the special pair of chlorophyll molecules drives the conversion of solar energy to chemical energy.[1−3] There have also been many studies of SB-CS in simpler molecular complexes, as chronicled in some recent reviews.[4−7] Intramolecular SB-CS has been reported in multipolar chromophores[8−13] while *inter*molecular SB-CS has been observed in multichromophore complexes such as covalently linked dimers[7,14−24] and trimers[25−27] of identical chromophores such as perylene diimide (PDI) derivatives.

SB-CS in PDI dimer complexes typically requires well-separated and weakly coupled chromophores in a polar solvent, where the asymmetric charge-transfer (CT) state is stabilized via solvent reorganization.[4−7] However, SB-CS has also been reported in closely spaced cofacial PDI and perylene complexes with relatively strong Coulomb coupling, in which the initial optically excited state is a bright Frenkel exciton (FE) delocalized over both chromophores. Coupling to similarly delocalized CT exciton (CTE) states, and subsequent relaxation along a slow-mode intermolecular vibrational coordinate usually results in excimer formation,[6,7,16,20,28−34] but in some cases, especially when the CT states are further stabilized by the presence of a polar solvent, the state relaxes to an asymmetric charge-separated cation/anion pair. Although almost exclusively observed in a polar environment, SB-CS has also been observed in cofacial PDI dimer complexes in low-polarity solvents like toluene.[19,20]

Like SB-CS, null aggregate (NA) formation requires coupling between Frenkel and CT excitons, driven by the electron (t_e) and hole (t_h) transfer integrals. In the limit of well-separated diabatic FE and CTE bands, such coupling can be treated perturbatively, resulting in CT-mediated energy transfer between chromophores, as described with an effective short-range exciton coupling, J_{CT}.[35−39] When such coupling interferes destructively with the Coulomb coupling, J_C, such that $J_C + J_{CT} \approx 0$, a NA results. Despite the close proximity between chromophores, the NA absorption spectrum resembles that of a monomer, especially with regard to the vibronic structure driven by the vinyl-stretching progression-forming mode.[35,36] NA formation has been observed in PDI foldamer complexes by Kaufman et al.,[40] in complexes of bis-adamantane linked anthracene derivatives by Nayak and Gopidas,[41] and in Greek-Cross pentacene[42] and PDI[17] dimers by Hariharan and co-workers.[43] Interestingly, several recent reports have linked SB-CS to NA formation.[17,26,44] A reduction of Coulomb coupling by increased linker length between two interacting chromo-

Received: October 12, 2023
Revised: November 22, 2023
Accepted: November 27, 2023
Published: January 2, 2024

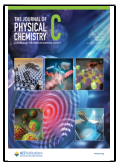

https://doi.org/10.1021/acs.jpcc.3c06785
J. Phys. Chem. C 2024, 128, 248−260

phores, or a favorable geometry such as the Greek Cross in which two transition dipole moments are essentially orthogonal, has been shown to enhance SB-CS *and* lead to NA formation.

In this work, we explore theoretically the relationship between SB-CS and NA formation in molecular dimer complexes with applications mainly to those based on PDI chromophores. Intermolecular coupling derives from the interacting molecular transition dipole moments (Coulomb coupling, J_C), which creates delocalized Frenkel excitons as well as molecular orbital overlap, which gives rise to the mixing between the Frenkel excitons and the CT excitons. The latter is governed by t_e and t_h, as well as the energy mismatch, $E_{CT} - E_{S1}$, between the diabatic CT energy E_{CT} (before solvent stabilization) and the local monomer excited state energy (E_{S1}). We show that both SB-CS and NA formation are optimized near a *null point*, defined as a degeneracy in either the lower- or upper-adiabatic exciton bands, and associated with certain set of electronic parameters $\{J_C, t_e, t_h, \text{and } E_{CT} - E_{S1}\}$. Such parameters are highly sensitive to the relative orientation between the two chromophores, so that a null point can be identified with a particular dimer geometry. It is important to emphasize that a null *point* is a quite general concept and does not require well-separated diabatic FE and CTE bands (as does a NA). In a π-stack containing many chromophores, a null point is identified with a flat (dispersionless) energy band. Oleson et al.[45] explored absorption and photoluminescence in large π-stacks (10 or more chromophores) of two phenyl-substituted PDI derivatives showing how they "straddle" a lower-band null point, resulting in hJ- and Hj-aggregates. Spectral simulations showed that at the null point, the resulting photoluminescence spectrum strongly resembles that of the monomer spectrum.

In what follows, we outline a recipe for efficient SB-CS in molecular dimers, where SB-CS is derived from fluctuations in solvent polarization. Beyond the Weller condition,[46] which states that the solvent-stabilized CT state should appear below the optical gap, two additional conditions are identified: (i) the presence of a null point and, just as important, (ii) lopsided electron and hole transfer integrals, such that $|t_e| \gg |t_h|$ or $|t_h| \gg |t_e|$. Together, these two conditions optimize the developing charge asymmetry in response to small fluctuations in the solvent-sourced electric field, which eventually lead to solvent-stabilized charge-separated states. We find that generally not all null points behave the same way: some are conducive to SB-CS, some are conducive to NA formation, and a smaller subset is conducive to both processes. We show that SB-CS is most likely launched from a null point in the lower band. However, a null point in the upper band may explain how SB-CS can occur in H-dimers with significant cofacial overlap, such as the PDI complexes reported in refs 19 and 20.

II. MODEL/HAMILTONIAN

Herein we treat molecular dimers containing two identical chromophores, such as the covalently bound PDI dimer complex in Figure 1, which has been shown to undergo SB-CS.[20] The two PDI chromophores are connected via a symmetry operation and interact Coulombically through their transition dipole moments as well as through orbital overlap, the latter giving rise to charge transfer.

For a molecular dimer, the electronic Hamiltonian consists of the sum,[35−37,47,48]

$$H = H_F + H_{CT} + H_{F-CT} \tag{1}$$

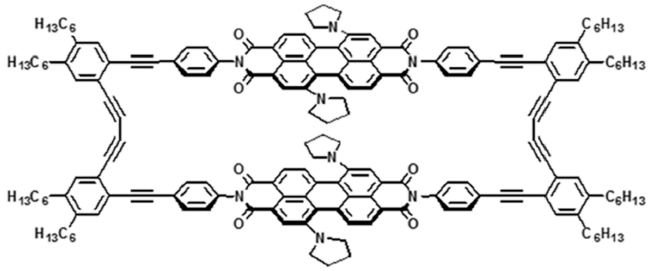

Figure 1. PDI dimer complex known as gPBI-cp. Reproduced from ref 20. Copyright 2022, ACS.

The first term accounts for the creation of Frenkel excitons and is given by,

$$H_F = E_{S_1} \sum_n |n^*\rangle\langle n^*| + J_C\{|1^*\rangle\langle 2^*| + |2^*\rangle\langle 1^*|\} \tag{2a}$$

where the state $|n^*\rangle$ indicates that the nth chromophore ($n = 1, 2$) hosts a local excitation (S_1), while the other chromophore remains unexcited (S_0). E_{S_1} is the monomer transition energy (taking the S_0 state as the zero of energy), and J_C is the Coulomb coupling between the two chromophores. Here, we assume that the local excitation is primarily a HOMO−LUMO excitation.

H_{CT} accounts for the energy of the intermolecular charge-transfer states, E_{CT},

$$H_{CT} = E_{CT}\{|1^+, 2^-\rangle\langle 1^+, 2^-| + |2^+, 1^-\rangle\langle 2^+, 1^-|\} \tag{2b}$$

The CT states $|1^+, 2^-\rangle$ and $|2^+, 1^-\rangle$ represent the two charge-separated (cation/anion) states. The cation consists of a half-filled HOMO, which is commonly referred to as a hole, while the anion has a filled HOMO orbital (no holes) and a half-filled LUMO, where the latter is referred to as an electron. In the electron/hole description, the local excitation therefore consists of one electron and one hole. It is important to note that E_{CT} in eq 2b is the energy of the CT states *before* significant stabilization induced by solvent reorganization (in polar solvents).

Finally, the coupling between the locally excited states and the CT states is given by,

$$\begin{aligned} H_{F\text{-}CT} = {} & t_e\{|1^*\rangle\langle 1^+, 2^-| + |2^*\rangle\langle 2^+, 1^-| + \text{h.c. }\} \\ & + t_h\{|1^*\rangle\langle 2^+, 1^-| + |2^*\rangle\langle 1^+, 2^-| + \text{h.c. }\} \end{aligned} \tag{2c}$$

where t_e and t_h are the electron and hole transfer integrals, respectively, defined by,

$$t_e \equiv \langle \text{LUMO}_1|\hat{h}|\text{LUMO}_2\rangle \tag{3a}$$

$$t_h \equiv -\langle \text{HOMO}_1|\hat{h}|\text{HOMO}_2\rangle \tag{3b}$$

where $\hat{h}$ is the complete one-electron Hamiltonian of the dimer complex. The negative sign in the hole transfer integral[35,47] accounts for the fact that moving a hole forward is equivalent to moving a (HOMO) electron backward.

The direct Coulomb coupling in H_F results in the two delocalized Frenkel exciton (FE) eigenstates,

$$|k\rangle_F \equiv 2^{-1/2}\{|1^*\rangle + e^{ik}|2^*\rangle\} \quad k = 0, \pi \tag{4}$$

with wave vector k, and with energies,

$$E_F(k) = E_{S_1} + J_C \cos(k) \tag{5}$$

The k wave vector notation is useful in comparing the dimer in this work to larger π-stacks ($N > 2$) with one molecular per unit

https://doi.org/10.1021/acs.jpcc.3c06785
J. Phys. Chem. C 2024, 128, 248−260

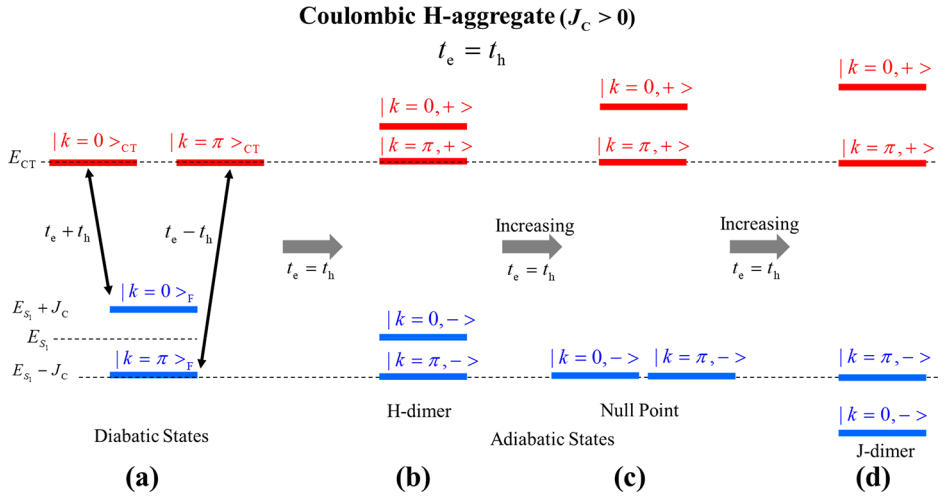

Figure 2. (a) Diabatic energy level scheme corresponding to a Coulomb-defined H-aggregate ($J_C > 0$) with FE-dominated lower-energy band. Coupling between diabatic states is represented by black arrows. (b–d) Activating t_e and t_h allows FE/CTE mixing which results in the adiabatic energy level scheme. In this example, the CT integrals are in-phase with $t_e = t_h$ so that only the $k = 0$ states couple (see eq 7). Increasing t_e or t_h, results in an H-dimer with reduced splitting in part b, a null point in part c, and a J-dimer in part d. In this figure and all that follows, a blue (red) energy level indicates a dominant FE (CT) component in the associated eigenfunction.

cell treated in previous works.[35−37,45] Here, translational symmetry leads to equivalent chromophores. (One could use other symmetry operations such as rotation or reflection without loss of generality.) The phase of the molecular orbitals are then chosen using translational symmetry, so that, for example $|HOMO_2\rangle$ is obtained by translating $|HOMO_1\rangle$. In addition, the transition dipole moment (TDM) corresponding to the HOMO−LUMO transition on chromophore 2, is obtained by translating the TDM of chromophore 1. As such, the $k = 0$ state in eq 4 carries all of the oscillator strength. The phase convention is also very important in defining the signs of the transfer integrals in eq 3.[35]

The two CT states in H_{CT} are degenerate, each with energy E_{CT}. Hence, they can also be expressed as delocalized CT exciton (CTE) states with wave vector k,

$$|k\rangle_{CT} \equiv 2^{-1/2}\{|1^+2^-\rangle + e^{ik}|2^+1^-\rangle\} \quad k = 0, \pi \tag{6}$$

The FE states in eq 4 and CTE states in eq 6 are diabatic states, as they are not yet mixed by $H_{F\text{-}CT}$. For a given value of k, mixing occurs via the matrix element,

$${}_F\langle k|H|k\rangle_{CT} = t_e + t_h \exp(ik) \tag{7}$$

Generally, the degree of mixing between the FE and CTE states determines the H- or J-nature of the short-range coupling.[35,36,45,49] The mixing is also a vital component of excimers and the intermediate state in singlet fission.[7] For a given value of k the diabatic Frenkel and CT states mix to form an adiabatic upper state, $|k,+\rangle$ and a lower state $|k,-\rangle$,

$$|k, \pm\rangle = c_F^{k,\pm}|k\rangle_F + c_{CT}^{k,\pm}|k\rangle_{CT} \quad k = 0, \pi \tag{8}$$

The corresponding energies are given by,

$$E_{k,\pm} = \frac{E_{CT} + E_F(k)}{2} \pm \sqrt{\frac{(E_{CT} - E_F(k))^2}{4} + t_e^2 + t_h^2 + 2t_e t_h \cos(k)} \tag{9}$$

For a π-stack with $N > 2$, the expression is similar except for an additional factor of 2 in front of the terms containing the electron and hole transfer integrals, as well as the appropriate modification of the Frenkel exciton band expression $E_F(k)$.[45]

Figure 2 illustrates the impact of the Frenkel/CT mixing on the energy level structure of a Coulomb-defined H-dimer ($J_C > 0$), highlighting the importance of the phase relationship between t_e and t_h. Here the diabatic upper and lower bands contain the CT and Frenkel excitons, respectively, as is usually the case in PDI dimers (blue and red levels indicate dominant FE and CT components, respectively). Before mixing (Figure 2a), the upper-band CT states are degenerate while the lower-band states depict the splitting characteristic of an H-aggregate. The figure shows that if the two CT integrals have the same sign and equal magnitude ($t_e = t_h$), only the $k = 0$ diabatic states will mix with each other (see eq 7), causing a significant reduction in the lower-band splitting as well as an induced H-like splitting in the upper band (Figure 2b). Further increases in t_e and t_h lead to degenerate lower-band states—a null point[35−37,45] as demonstrated in Figure 2c—beyond which the order of the energy levels is reversed, resulting in a J-dimer in Figure 2d. Hence, FE/CTE mixing with in-phase CT integrals promotes a J-like behavior in the lower band. Moreover, it is easy to appreciate that changing the relative sign between the CT integrals ($t_e = -t_h$) causes only the $k = \pi$ states to mix, resulting in enhanced H-like splitting in the lower band, with no null point or J-dimer conversion. Details of the H- and J-promoting nature of the FE/CTE mixing can be found in several works.[35−37,45] As we will see, the intricate interplay between Coulomb coupling and CT-mediated coupling plays a major role in SB-CS as well as NA formation.

Finally, we consider the symmetry-breaking Hamiltonian, H'. Here, we attribute symmetry-breaking to the small energetic fluctuations, δE, arising from the electric fields associated with changes in the polarizable environment due, for example, to polar solvent motion. Such electric fields couple directly to the excited-state dipole moment of the dimer complex which arises from the CT component. The associated Hamiltonian is,

$$H' = \delta E\{|2^+1^-\rangle\langle 2^+1^-| - |1^+2^-\rangle\langle 1^+2^-|\} \tag{10}$$

https://doi.org/10.1021/acs.jpcc.3c06785
J. Phys. Chem. C 2024, 128, 248−260

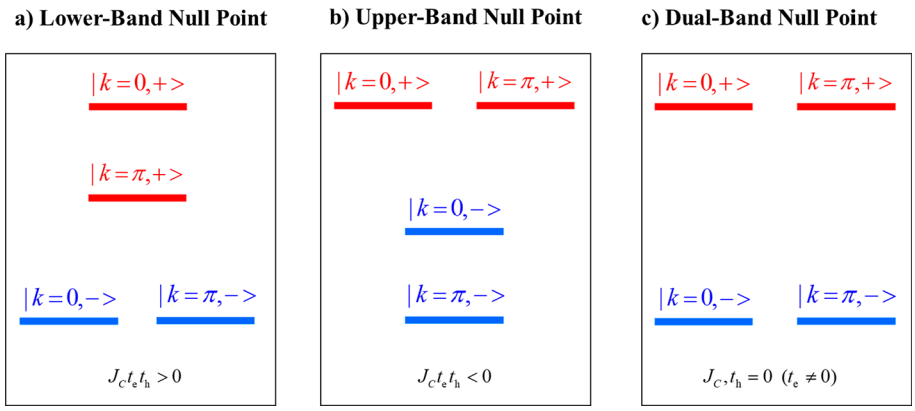

Figure 3. Adiabatic energy levels corresponding to null points in (a) the lower band, (b) the upper band, and (c) both the lower and upper bands. The phase relationships among the electronic coupling parameters are reported at the bottom of each panel. In parts a and b, it is assumed that $J_C > 0$ so that the $k = 0$ state is the higher of the split levels (as in an H-aggregate). In part c, one can also have J_C, $t_e = 0$ if t_h is dominant. Blue (red) energy level indicates a dominant FE (CT) component in the associated eigenfunction.

In a polar solvent, δE fluctuates about zero, with a standard deviation that increases with solvent polarity. In accord with eq 10, positive δE values stabilize the $|1^+2^-\rangle$ state, while negative values stabilize the $|2^+1^-\rangle$ state. H' couples adiabatic states in eq 8 with different values of k, thereby allowing effective SB-CS as will be shown below.

In what follows, we assume an initial fluctuation $\delta E > 0$ so that SB-CS results in a solvent-stabilized $|1^+2^-\rangle$ state. In addition, δE is taken to be less than approximately 10^{-3} eV, much smaller than typical values of t_e, t_h and J_C in PDI dimers. As the dimer develops charge asymmetry (and therefore a dipole moment) in response to H', it creates a reaction field which acts to further orient the surrounding solvent molecules, which, in turn, increases the electric field on the dimer, causing increased stabilization and so on. This process continues until the solvent reorganization is complete, at which point the lowest-energy state of the dimer is dominated by the CT component, with the stabilized energy denoted as $E_{CT}(sol)$. For PDI dimer complexes in a polar solvent, $E_{CT}(sol)$ can be several hundred meV lower than the energy of the initial, optically excited state (before solvent reorganization).[4,17]

III. RESULTS

In this section, we show how both SB-CS and NA formation are related to the presence of null points. A null point occurs when the values of J_C, t_e, t_h and $E_{CT} - E_{S_1}$ are such that degeneracies occur in the lower band ($E_{k=0,-} = E_{k=\pi,-}$), the upper ($E_{k=0,+} = E_{k=\pi,+}$) band or both, as indicated in Figure 3. Such degeneracies make the dimers extremely susceptible to the symmetry-breaking fluctuations induced by H' in eq 10. Prior work by our group was confined to NA formation induced by null points in the lower-energy (FE-dominated) band.[35,36,45] Here, we introduce a general theoretical framework with which to analyze mainly the impact of both lower- and upper-band null points on SB-CS. We also show how our prior results on NA formation are neatly accounted for within the current approach. An interesting question arises as to whether a given null point can promote *both* SB-CS and NA formation.

To determine a lower-band null point as depicted in Figure 3a, we set $E_{k=0,-} = E_{k=\pi,-}$ Subsequent use of eq 9 and some tedious algebra results in the expression that defines the lower-band null point in a molecular dimer,

$$-J_C^2(t_e^2 + t_h^2) + 4t_e^2t_h^2 = 2t_et_hJ_C(E_{CT} - E_{S_1}) \tag{11}$$

In addition, the product of the electronic couplings must be positive,

$$J_Ct_et_h > 0 \qquad \text{lower-band null pt} \tag{12a}$$

According to eq 12a, for a Coulomb-defined H-aggregate ($J_C > 0$), the product t_et_h must be positive, (i.e., t_e and t_h must be in-phase) in order to realize a null point in the lower band. If $J_C < 0$ then t_et_h must be negative.

For the upper-band null point, setting $E_{k=0,+} = E_{k=\pi,+}$ also leads to eq 11, although the phase condition for the electronic couplings reverses, leading to,

$$J_Ct_et_h < 0 \qquad \text{upper-band null pt} \tag{12b}$$

An upper-band null point is depicted in Figure 3b. eq 11 with the phase relations in eqs 12a and 12b reveal a simple relationship between the lower-band and upper-band null points: If a null point in the lower band occurs for the values $\{J_C, t_e, t_h, E_{CT} - E_{S_1}\}$ then there is also a null point in the upper-band for the values, $\{J_C, t_e, -t_h, -(E_{CT} - E_{S_1})\}$, $\{J_C, -t_e, t_h, -(E_{CT} - E_{S_1})\}$ and $\{-J_C, t_e, t_h, -(E_{CT} - E_{S_1})\}$.

There is also the interesting limiting case in eq 11 where the product $J_Ct_et_h = 0$, realized when $J_C = 0$ and one of the transfer integrals (t_e or t_h) is nonzero. In this case, there is degeneracy in *both* bands - a *dual*-band null point, as demonstrated in Figure 3c. The case can be understood directly from the energy level diagram in Figure 2a. When $J_C = 0$, both the upper and lower *diabatic* bands are doubly degenerate. The degeneracy is maintained in the adiabatic limit when $|t_e + t_h|$ and $|t_e - t_h|$ are equal, or, equivalently, when one of the CT integrals is zero. (The case where both t_e and t_h are zero is a trivial one since no coupling at all exists between the diabatic states.)

In what follows, we further investigate SB-CS and NA formation in molecular dimers using the electronic coupling parameters based on typical chromophores like PDI, where $|J_C|$, $|t_e|$ and $|t_h|$ are usually less than about 0.1 eV. We begin with the most general case, where all of the electronic coupling parameters are nonzero. Generally, in closely spaced dimers the Coulomb coupling J_C is significant, with the important exceptions being the "Greek Cross" configuration,[17,42] where the two molecular transition dipole moments form approximately a 90-degree angle, as well as configurations with parallel,

https://doi.org/10.1021/acs.jpcc.3c06785
J. Phys. Chem. C 2024, 128, 248−260

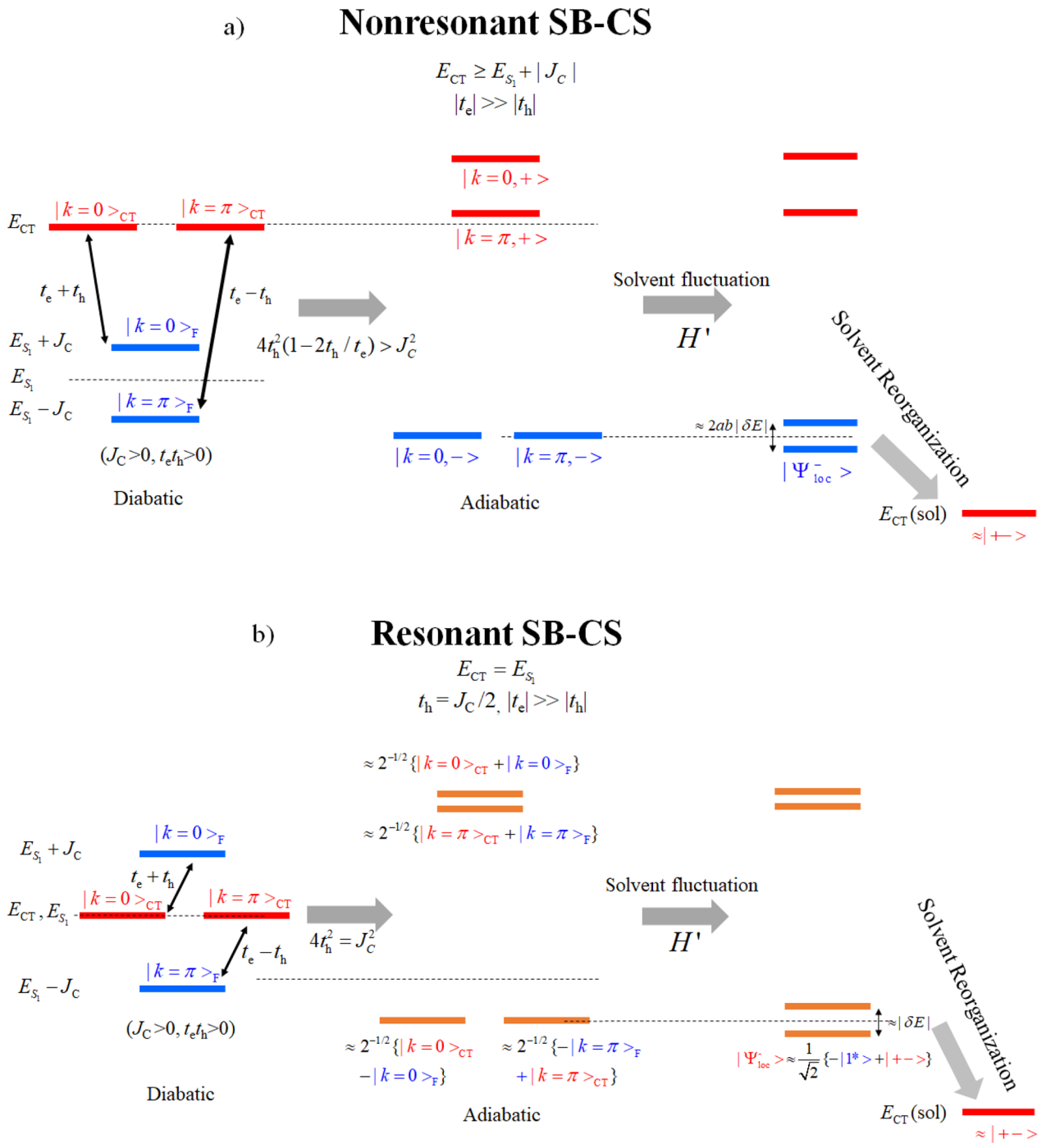

Figure 4. (a) Nonresonant and (b) resonant SB-CS for a molecular dimer with $J_C > 0$, beginning with the diabatic states (left) with electronic couplings represented by the black arrows. The adiabatic states (center) are formed after activating (in-phase) t_e and t_h with dominant t_e. The degenerate adiabatic states, which define a lower-band null point, are initially split by a solvent fluctuation.(right) Subsequent solvent reorganization results in the lowest-energy state with dominant, asymmetric CT character (+−). (far right) The antistabilized, (−+)-dominated state is not shown but increases with energy as the solvent reorganizes.

slipped transition dipole moments in the vicinity of the magic angle. The CT integrals t_e and t_h are far more sensitive than J_C to intermolecular orientation and can change sign upon molecular slip distances of the order of a bond-length.[50] Finally, in PDI crystals, the diabatic CT energy is typically greater than the molecular S_1 energy, $E_{CT} - E_{S_1} \geq 0$, but depends sensitively on the packing geometry, increasing with nearest-neighbor distance as the Coulomb binding energy diminishes.[51] In a prior work,[45] we obtained accurate spectral simulations for the crystal phases of several PDI derivatives using $E_{CT} - E_{S_1} \approx 0.1$ eV. Hence, in all that follows we take $E_{CT} - E_{S_1} \geq 0$.

Lower-Band SB-CS. Although null points can occur in either band, we expect SB-CS to be most efficiently launched from a null point in the lower-energy band, which is increasingly dominated by the FE component as $E_{CT} - E_{S_1}$ increases. Since the bulk of the oscillator strength is contributed by the FE component, the lower-energy band is directly optically excited.

https://doi.org/10.1021/acs.jpcc.3c06785
J. Phys. Chem. C 2024, 128, 248−260

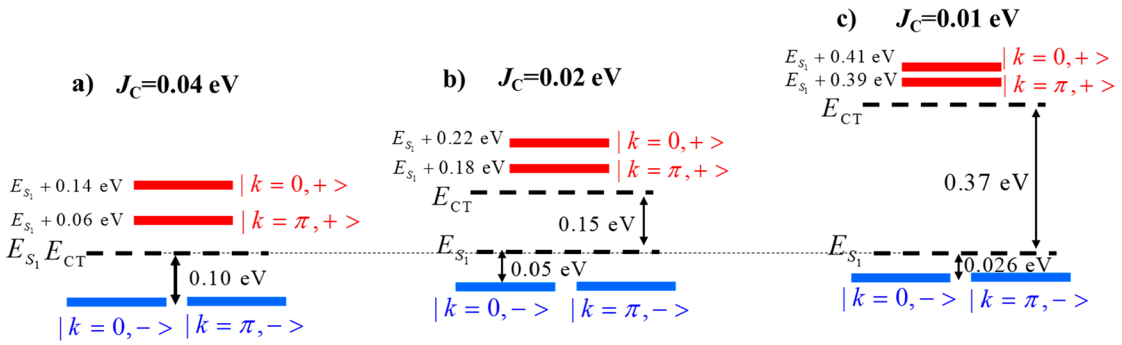

Figure 5. Adiabatic energy level schemes for lower-band null points in Coulomb-defined H-dimers ($J_C > 0$) for several values of J_C. In part a, $E_{CT} \approx E_{S1}$ (resonant) while parts b and c represent nonresonant cases, with $E_{CT} > E_{S1}$. In all cases, the electron CT integral is dominant, $t_e = 0.1$ eV, being five times larger than the hole integral, $t_h = 0.02$ eV. Blue (red) levels indicate a dominant FE (CTE) component.

SB-CS is but one fate of the excited state, as it may also decay via singlet exciton fission or excimer formation.[6,7]

To obtain lower-band SB-CS the adiabatic states, $|k = 0,-\rangle$ and $|k = \pi,-\rangle$, must effectively mix together under the influence of H' in eq 10 to form charge-asymmetric states. This occurs most efficiently when,

$$|E_{k=0,-} - E_{k=\pi,-}| \ll |ab\delta E| \tag{13}$$

where $-ab\delta E$ is the matrix element of H' connecting the $|k = 0,-\rangle$ and $|k = \pi,-\rangle$ adiabatic states. Here, we have introduced a more convenient notation, $a \equiv c_{CT}^{k=0,-}$ and $b \equiv c_{CT}^{k=\pi,-}$, with the wave function coefficients defined in eq 8 and with $ab > 0$ taken without loss of generality. The condition (13) is readily satisfied at or near a null point for degenerate wave functions having large CT components, a and b.

Under condition (13), the mixing is well-described by degenerate perturbation theory, resulting in the (zero-order) localized wave functions,

$$|\Psi_{loc}^{+}\rangle = \frac{1}{\sqrt{2}}\{|k = 0, -\rangle - |k = \pi, -\rangle\} \tag{14a}$$

$$|\Psi_{loc}^{-}\rangle = \frac{1}{\sqrt{2}}\{|k = 0, -\rangle + |k = \pi, -\rangle\} \tag{14b}$$

Corrected to first-order, the energies of the states in eq 14 are $E_{loc}^{\pm} = E_{n.p.} \pm ab\delta E$, where $E_{n.p.}$ is the null point energy ($=E_{k=0,-} = E_{k=\pi,-}$). Since $\delta E > 0$, the state $|\Psi_{loc}^{-}\rangle$ in eq 14a is more stable. The charge asymmetry within the state $|\Psi_{loc}^{-}\rangle$ is given by,

$$\eta_{CT} \equiv |\langle +-|\Psi_{loc}^{-}\rangle|^2 - |\langle -+|\Psi_{loc}^{-}\rangle|^2 \tag{15}$$

where we have introduced the more user-friendly notation, $|+-\rangle \equiv |1^+2^-\rangle$ and $|-+\rangle \equiv |2^+1^-\rangle$. Substituting eq 8 and eq 14b into eq 15 gives $\eta_{CT} = ab$. Hence, achieving the largest charge asymmetry in $|\Psi_{loc}^{-}\rangle$ is equivalent to maximizing the right-hand side of eq 13.

Equation 13 shows that solvent fluctuations are most effective in creating charge-asymmetric states at or near a null point for degenerate wave functions having large CT components, a and b. This immediately disqualifies the case where $|t_e|$ and $|t_h|$ are comparable. For example, when $J_C > 0$ and $t_e = t_h$, the $k = \pi$ diabatic states will not mix at all (see Figure 2a and eq 7) so that $b \equiv c_{CT}^{k=\pi,-} = 0$ and the perturbation H' cannot induce any mixing ($ab = 0$ in eq 13) *even at a null point*. Hence, the null point in Figure 2c cannot result in SB-CS. A similar argument applies when $J_C < 0$ and $t_e = -t_h$, whereupon $a \equiv c_{CT}^{k=0,-} = 0$. Hence, for SB-CS to be initiated at (or near) a null point, $|t_e|$ and $|t_h|$ need to differ substantially so that the product ab is maximized.

Referring to Figure 2a, large and comparable values of a and b result when the coupling between the $k = 0$ states is similar to the coupling between the $k=\pi$ states, i.e., when $|t_e + t_h| \approx |t_e - t_h|$, and when such coupling is sufficiently large compared to $|J_c|$. This is accomplished when either $|t_e| \gg |t_h|$ or $|t_h| \gg |t_e|$, with the magnitude of the dominant coupling, e.g., $|t_e|$, comparable to or larger than $|J_C|$.

In summary, null points with lopsided electron and hole transfer integrals lead to strongly asymmetric local states in response to the solvent-induced fluctuations H'. However, to proceed to full-fledged SB-CS the energy of the solvent-stabilized state, $E_{CT}(sol)$ ($<E_{CT}$), which results from complete solvent reorganization, must be lower than the energy of the initially optically excited exciton, such that the Gibbs energy for charge separation, ΔG_{CS} is negative. This condition was originally pointed out by Weller.[46] Typically, ΔG_{CS} is less than -0.2 eV for efficient SB-CS in PDI chromophores.[17] A strong driving force for SB-CS ensures that it occurs sufficiently rapidly, typically in the range 1−100 ps,[4,5] to outcompete other relaxation process.

Figures 4a and 4b schematically depict lower-band SB-CS in a Coulomb-defined H dimer ($J_C > 0$) so that a null point requires t_e and t_h to be in-phase ($t_e t_h > 0$), see eq 12a. The figure portrays the diabatic energy level scheme on the left and proceeds through to the solvent-stabilized charge-asymmetric state on the right. Figure 4a pertains to the nonresonant regime where $E_{CT} - E_{S_1} > |J_C|$, i.e., well-separated diabatic FE and CTE bands. Figure 4b shows the resonant regime, where $E_{CT} - E_{S_1} \approx 0$; i.e., the local excited state is resonant with the diabatic CT state. Similar diagrams can be constructed for Coulomb-defined J-aggregates ($J_C < 0$).

The nonresonant and resonant SB-CS processes outlined in Figures 4a and 4b assume a dominant electron transfer integral, $|t_e| \gg |t_h|$. In this limit eq 11, under condition (12a), reduces to the form

$$E_{CT} - E_{S_1} \approx \frac{(4 - J_C^2/t_h^2)}{2|J_C/t_h|}|t_e|, \quad |t_e| \gg |t_h|, \quad J_C t_e t_h > 0 \quad \text{lower band} \tag{16}$$

Equation 16 can be more easily used to identify null points in the lower band. The equation shows that in order to obtain null points for $E_{CT} - E_{S_1} \geq 0$, one must have $J_C^2 \leq 4t_h^2$, so that, overall, $|J_C| = 2|t_h| \ll |t_e|$ i.e. relatively weak values of $|J_C|$ and $|t_h|$ relative to $|t_e|$. The equality, $J_C^2 = 4t_h^2$, corresponds to the resonant regime, $E_{CT} = E_{S_1}$ depicted in Figure 4b. Importantly, eq 16 also shows

https://doi.org/10.1021/acs.jpcc.3c06785
J. Phys. Chem. C 2024, 128, 248−260

that a given null point depends only on three parameters, $E_{CT} - E_{S_1}$, $|t_e|$ and the ratio $|J_c/t_h|$.

In the nonresonant regime of Figure 4a, the condition, $E_{CT} - E_{S_1} \geq J_C$, is maintained as long as $J_C^2 \leq 4t_h^2(1 - 2t_h/t_e)$, where eq 11 was required to obtain the small correction of order t_h/t_e. Because $J_C > 0$ in both Figure 4a and Figure 4b, t_e and t_h also need to be in phase (same sign) so that the coupling among the diabatic $k = 0$ states is slightly greater than that between the $k=\pi$ states, as can be appreciated from the left side of Figure 4. Figures 4a and 4b also show that the reaction to an initial fluctuation H' results in only a small splitting, $2ab\delta E$, between the states in eq (14). However, the induced charge asymmetry creates a reaction field that leads to additional alignment of the polar environment, which in turn amplifies subsequent δE, and so on. When solvent reorganization is complete, the stabilized state, $|\Psi_{loc}^-\rangle$, is entirely dominated by the CT component with energy $E_{CT}(sol)$, as shown in the figures. For efficient SB-CS, the state should be at least as stable as E_{S1}.[46]

To better illustrate SB-CS-inducing null points, we consider a dimer with $J_C > 0$ (a Coulomb- defined H-dimer) with an electron transfer integral, $t_e = 0.1$ eV, five times larger than the hole transfer integral, $t_h = 0.02$ eV. Figure 5a-c shows the adiabatic energy level diagrams at the null point for (a) $J_C = 0.04$ eV (resonant), (b) $J_C = 0.02$, and (c) $J_C = 0.01$ eV. According to eq 11, the null conditions in Figure 5a−c are reached when $E_{CT} - E_{S_1} = -0.004$, 0.148, and 0.374 eV, respectively, which agrees well with the values of 0.0, 0.15, and 0.375 eV from eq 16. (We continue to refer to case a as "resonant" despite the slight mismatch of 0.004 eV between E_{CT} and E_{S1} which vanishes as $|t_e/t_h|$ increases.) Figure 5 shows that $E_{CT} - E_{S_1}$ increases to maintain a null point as J_C diminishes, in agreement with the predictions of eq 16. Increasing $E_{CT} - E_{S_1}$ also results in decreasing CTE character of the degenerate band-bottom states and hence we expect less charge asymmetry for the smaller values of J_C. We point out that the null point is preserved—i.e., the lower level remains degenerate—when J_C is reversed in sign to make a Coulomb-defined J-aggregate, as long as either t_h (or t_e) also changes sign so as to maintain the phase of the product, $J_C t_e t_h > 0$.

Based only on the energy level diagrams in Figure 5, it is not clear whether the null points are also SB-CS conducive. For this, we need to confirm the wave function asymmetry, η_{CT} from eq 15, after application of the small fluctuation H' in eq 10. Figure 6a shows how the CT admixtures, $\langle +-|\Psi_{loc}^-\rangle|^2$ and $|\langle -+|\Psi_{loc}^-\rangle|^2$ vary as a function of $E_{CT} - E_{S_1}$ for the J_C values in Figure 5 and for $\delta E = 10^{-3}$ eV. Null points are clearly identified by the sharp increase in η_{CT}, which is the difference between the red and black curves.

When $J_C = 0.04$ eV the null point appears near $E_{CT} - E_{S_1} = 0$ (resonant case). Here, the charge asymmetry peaks at $\eta_{CT} \approx 0.5$, with the admixture of the $|+-\rangle$ state reaching 50%, while the $|-+\rangle$ component plummets to almost zero. The remaining 50% of the local wave function is taken up by the Frenkel exciton components (not shown), which supply the oscillator strength for optical excitation. As J_C decreases further, null point maintenance requires higher values of $E_{CT} - E_{S_1}$, which coincides with a reduction in the $|+-\rangle$ admixture in the lower-band as well as a decrease in η_{CT}, making such null points less SB-CS conducive.

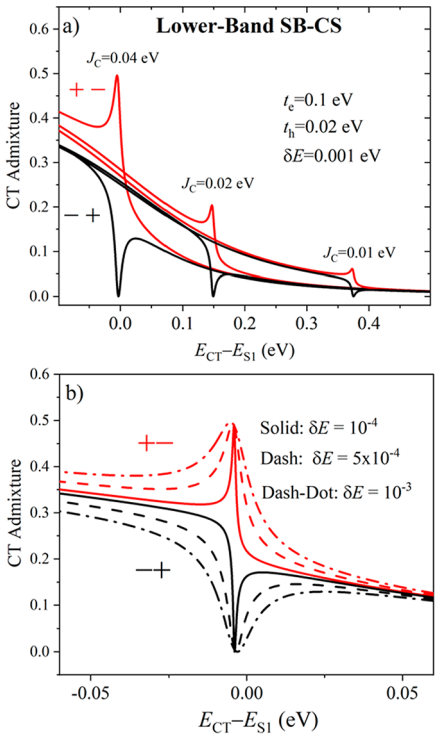

Figure 6. (a) CT admixtures, $|\langle +-|\Psi_{loc}^-\rangle|^2$ (red) and $|\langle -+|\Psi_{loc}^-\rangle|^2$ (black), in the localized charge-asymmetric wave function as a function of $E_{CT} - E_{S_1}$ for Coulomb-defined H-dimers. The fluctuation energy is $\delta E = 0.001$ eV. (b) CT admixtures vs $E_{CT} - E_{S_1}$, for $J_C = 0.04$ eV for several values of δE. In all cases, $t_e = 0.1$ eV $= 5t_h$.

From Figure 6, one can conclude that the most efficient lower-band SB-CS occurs at null points corresponding to $|E_{CT} - E_{S_1}|$ less than approximately 0.1 eV. This ensures substantial charge asymmetry, η_{CT}, as well as a sufficiently large FE component for optical absorption. The figure also shows that η_{CT} surrounding each null point decays to near zero fairly quickly, defining a narrow "line width". As expected, the latter increases with δE as demonstrated in Figure 6b, so that SB-CS can occur over a wider range of $|E_{CT} - E_{S_1}|$.

We now show that charge asymmetry can be dramatically enhanced for $|E_{CT} - E_{S_1}|$ values surrounding the null point as J_C and t_h are both reduced *while maintaining their ratio*. We consider the near resonance regime where $|J_c/t_h| = 2$. Figure 7 shows how the charge asymmetry responds as J_C and t_h approach very small values of the order of δE, while t_e is maintained at 0.1 eV throughout. Also shown (dotted curves) is the theoretical limit of $J_C = t_h = 0$.

For the largest value of J_C ($=2t_h = 0.04$ eV, solid curves) the null point on the lower-band is clearly observed for $E_{CT} - E_{S_1}$ near zero, with η_{CT} near 0.5 as in Figure 6a. As J_C (and therefore t_h) is further reduced, the asymmetry increases substantially about the null point, $E_{CT} - E_{S_1} = 0$, extending well into the regions of positive and negative $E_{CT} - E_{S_1}$. When J_C and t_h approach δE, the (+,−) and (−,+) CT admixtures approach the dotted red and black curves, respectively, in Figure 7a, which correspond to the limit $J_C = t_h = 0$. Here, the asymmetry is quite substantial out to $E_{CT} - E_{S_1} = 0.2$ eV.

The behavior observed in Figure 7a arises because the change in energy, $\Delta E \equiv |E_{k=0,-} - E_{k=\pi,-}|$, surrounding the null point

https://doi.org/10.1021/acs.jpcc.3c06785
J. Phys. Chem. C 2024, 128, 248−260

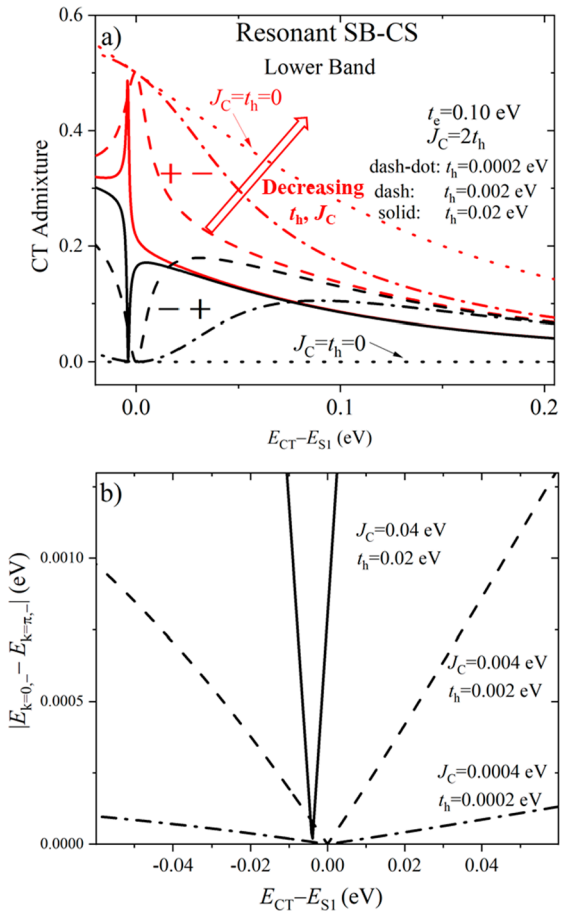

Figure 7. (a) CT admixtures, $|\langle +-|\Psi^{-}_{loc}\rangle|^2$ (red) and $|\langle -+|\Psi^{-}_{loc}\rangle|^2$ (black), in the localized, charge asymmetric wave function as a function of $E_{CT} - E_{S_1}$ for Coulomb-defined H-dimers with $J_C = 2t_h$ and for several values of t_h, In all cases, t_e = 0.1 eV and $\delta E = 10^{-4}$ eV. (b) ΔE as a function of $E_{CT} - E_{S_1}$ for the case for the parameter sets from part a evaluated before application of the fluctuation. Null points correspond to $\Delta E = 0$.

becomes less sensitive to $E_{CT} - E_{S_1}$ as J_C and t_h decrease, making the surrounding region more susceptible to small fluctuations, δE. This can be appreciated from Figure 7b, which shows ΔE vs $E_{CT} - E_{S_1}$ for the values of J_C and t_h from Figure 7a. The range at which eq 13 is satisfied becomes broader as J_C and t_h decrease. Overall, Figure 7 shows why SB-CS is more likely to be observed in dimers with small Coulombic couplings, such as the Greek Cross geometry.[17]

Null Aggregates. In this subsection, we briefly consider null aggregates, which have recently been linked to efficient SB-CS in PDI dimers.[17,26] As we will see, although NAs and SB-CS require null points, not all null points share the same characteristics. Some, as we have already seen, lead to efficient SB-CS while others lead to NA formation. As shown below, a small subset of null points lead to NA formation and mild SB-CS. There are also null points that lead to neither SB-CS or NAs.

NAs are created at null points in the lower-energy band, in the limit of well-separated diabatic CTE and FE bands. As shown earlier[35−37] in this limit the admixture of the CT states in the lower-band degenerate states is small, so that their inclusion can be treated using second-order perturbation theory. In this manner, FE/CTE mixing gives rise to short-range exciton coupling, J_{CT}, which interferes with the Coulomb coupling, J_C. When J_{CT} and J_C have opposite signs and similar magnitudes, they effectively cancel out, yielding NAs with spectral properties that are very similar to individual monomers.

Well-separated diabatic FE and CTE bands occur when $E_{CT} - E_{S_1} \gg |J_c|$. For general null point formation in the lower energy band, this inequality is consistent with eqs 11 and 12a when the term $4t_e^2t_h^2$ dominates the left-hand-side, i.e., when

$$4t_e^2t_h^2 \gg J_C^2(t_e^2 + t_h^2) \tag{17}$$

Rearranging eq 11 under condition (17) gives

$$E_{CT} - E_{S_1} \approx \frac{2t_et_h}{J_C} \qquad J_Ct_et_h > 0 \tag{18}$$

as the condition for NA formation. Equation 18 can be rewritten as,

$$J_C + J_{CT} \approx 0 \qquad |J_C|, |t_e|, |t_h| \ll E_{CT} - E_{S_1} \tag{19}$$

where, the CT-induced, short-range exciton coupling is given by[35−37]

$$J_{CT} \equiv \frac{-2t_et_h}{E_{CT} - E_{S_1}} \tag{20}$$

Equation 20 shows that J_{CT} promotes J-aggregation ($J_{CT} < 0$) when t_e and t_h are in-phase and promotes H-aggregation ($J_{CT} > 0$) when t_e and t_h are out-of-phase. According to eq 19 within a NA, J_C and J_{CT} must have opposite signs. A NA is therefore a manifestation of contrasting H and J influences which effectively cancel out, yielding monomer-like spectral behavior.[35−37] The condition accompanying eq 19 follows from eqs 17 and 18 and justifies a perturbative treatment of NA formation as was done in refs 35−37.

With the definition of a NA firmly in hand, we now revisit the null points in Figure 6a to see if they correspond to NAs. The null point in Figure 6a for the resonant case, $E_{CT} - E_{S_1} = 0$, cannot qualify as NA formation since eq 19 is undefined—the diabatic bands are not separated at all; see Figure 4b. Moreover, on resonance, both the lower and upper adiabatic bands have comparable FE components so that each band receives roughly half of the oscillator strength, making the absorption spectrum quite different from that of the monomer.

The nonresonant null points in Figure 6a are much more in line with NAs. For J_C = 0.02 and 0.01 eV, null points occur when $E_{CT} - E_{S_1}$ is 0.148 and 0.374 eV, respectively. Compared with the approximate values of 0.2 and 0. 4 eV obtained from the NA condition in eq 19, agreement is fairly good and improves with increasing $E_{CT} - E_{S_1}$. At such points, the FE component is dominant and the absorption spectrum will closely resemble that of the monomer. However, Figure 6a also shows that increasing $E_{CT} - E_{S_1}$ leads to diminishing charge asymmetry, with $\eta_{CT} \approx 0.2$ and 0.05 when J_C = 0.02 and 0.01 eV respectively. Hence, it may be possible to have approximate NA formation with SB-CS at (nonresonant) null points in the lower band, although SB-CS is not optimal.

Importantly, since eq 19 is derived directly from eq 11, it makes no restrictions on the relative magnitudes of t_e and t_h; they do not have to be lopsided as required for SB-CS. Hence, there exists another subclass of NA-forming null points distinct from those in Figure 6, in which t_e and t_h are *not* lopsided—those with comparable values of the CT integrals, $t_e \approx t_h$, such as in Figure 2c. In the limit that $t_e = t_h$, the null points from eq 19—or even

https://doi.org/10.1021/acs.jpcc.3c06785
J. Phys. Chem. C 2024, 128, 248−260

from the more general null point equation, eq 11—will not result in any wave function asymmetry after the application of the symmetry-breaking solvent fluctuation in eq 10. This is because according to eq 7 when $t_e = t_h$, the $k = \pi$ diabatic states do not couple at all so that the product ab in eq 13 is exactly zero. Similar conclusions are drawn when $t_e = -t_h$.

Upper-Band SB-CS. We conclude our analysis by considering null points in the upper-band, as depicted in Figure 3b, and their potential for SB-CS. Upper-band SB-CS may explain the curious observation of SB-CS in cofacially oriented perylene[16,23] and PDI[19,20,24] dimers (see Figure 1), where the absorption spectrum reveals H-aggregation through an attenuation of the first vibronic peak relative to the second. The spectra indicate an FE dominated lower-band ($E_{CT} - E_{S_1} > 0$) with an H-like energy level ordering.

Upper-band SB-CS requires a condition analogous to eq 13 but involving the two upper-band adiabatic states. However, when E_{CT} exceeds E_{S1} the upper-band states, $|k = 0,+\rangle$ and $|k = \pi,+\rangle$, become dominated by their CT components, a and b, so that generally the asymmetry η_{CT} in the localized state, $|\Psi_{loc}\rangle = 2^{-1/2}\{|k = 0,+\rangle + |k = \pi,+\rangle\}$ exceeds the asymmetry values associated with lower-band SB-CS. However, the increase in η_{CT} comes at the expense of a diminishing FE component, making the absorption cross-section significantly smaller in the upper vs lower-band. In addition, SB-CS in the upper-band must compete with rapid interband relaxation in the lower-band.

In analyzing upper-band SB-CS we continue to assume a dominant electron transfer integral, so that the upper-band null condition in Equations 11 and 12b can be rewritten as,

$$E_{CT} - E_{S_1} \approx \frac{(J_C^2/t_h^2 - 4)}{2|J_C/t_h|}|t_e|, \quad |t_e| \gg |t_h|, \quad J_C t_e t_h < 0 \quad \text{upper-band} \tag{21}$$

In contrast to eq 16, eq 21 shows that positive values for $E_{CT} - E_{S_1}$ require $|J_C| \geq 2|t_h|$. Note that because $J_C t_e t_h < 0$, the SB-CS inducing null points in eq 21 apply for Coulomb-defined H aggregates ($J_C > 0$) when t_e and t_h have opposite signs, i.e., out-of-phase, with $t_e t_h < 0$. For Coulomb-defined J-aggregates ($J_C < 0$), t_e and t_h must be in-phase ($t_e t_h > 0$).

To demonstrate upper-band symmetry breaking, we return to the Coulomb-defined H-dimer ($J_C > 0$) considered previously, with an electron transfer integral, $t_e = 0.1$ eV, five times larger (in magnitude) than the hole transfer integral, $t_h = -0.02$ eV. (Note the sign change in t_h compared to the lower-band null points in Figure 5 is required by eq 12b). We consider three values of the Coulomb coupling, $J_C = 0.04$, 0.06, and 0.08 eV. The first value of J_C corresponds to resonant SB-CS, where $J_C = 2|t_h| = 0.04$ eV, the same as in Figure 5a, while the second and third values lead to nonresonant SB-CS. According to eq 21 the null points occur when $E_{CT} - E_{S_1} = 0$, 0.083, and 0.15 eV, which agrees well with the exact values of 0.004, 0.089, and 0.158 eV from eq 11.

Figure 8 displays the energy level diagrams for just the extreme values, $J_C = 0.04$ and 0.08 eV at their respective null points. Interestingly, the splitting of the H-like lower-band remains unaffected by Frenkel/CT mixing, adhering to the diabatic value of $2J_C$ in both cases,

$$E_{k=0,-} - E_{k=\pi,-} = 2J_C \tag{22}$$

This is a rigorous result that can be derived from eq 9 when $E_{k=0,+} = E_{k=\pi,+}$. Figure 8 also shows that the upper-band adiabatic states shift to significantly higher energies with increasing J_C.

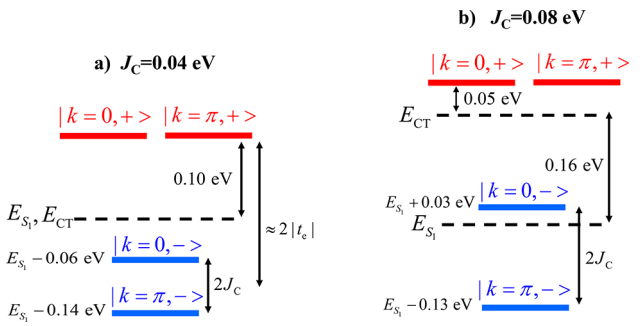

Figure 8. Adiabatic energy level schemes for upper-band null points in Coulomb-defined H-dimers ($J_C > 0$), for two values of J_C. Part a represents the resonant case, $E_{CT} \approx E_{S1}$, while parts b is nonresonant with E_{CT} substantially larger than E_{S1}. Note that the energy level scheme in part a is just the inverted version of the lower-band resonant case in Figure 5a. The splitting of the lower band remains at $2J_C$ in both parts a and b. In all cases, the electron CT integral is dominant, with $t_e = 0.1$ eV, with the hole integral, $t_h = -0.02$ eV. Note the product, $t_e t_h$ is now negative as opposed to Figure 5.

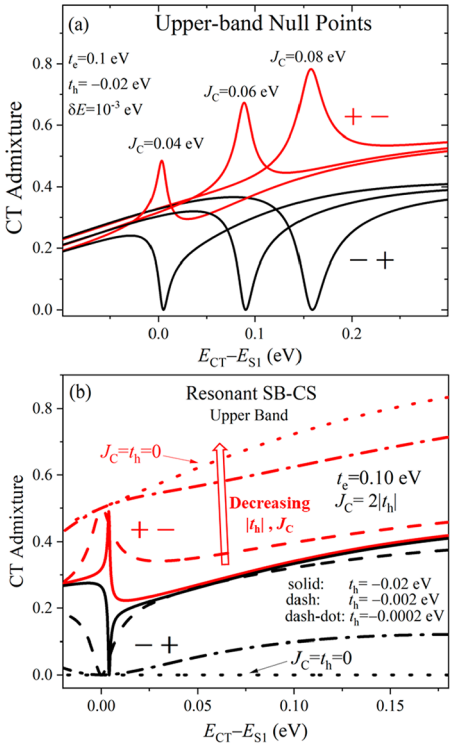

Figure 9. (a) CT admixtures, $|\langle +-|\Psi_{loc}^-\rangle|^2$ (red) and $|\langle -+|\Psi_{loc}^-\rangle|^2$ (black), in the localized, charge-asymmetric state in the upper band as a function of $E_{CT} - E_{s_1}$ for Coulomb-defined H-dimers for several values of J_C (>0). In all cases, $t_e = 0.1$ eV and t_h=−0.02 eV with δE = 0.001 eV. (b) CT admixtures as a function of $E_{CT} - E_{s_1}$ for the resonant case ($J_C = -2t_h$) and for several values of t_h. In all cases, $t_e = 0.1$ eV and $\delta E = 10^{-4}$ eV.

Figure 9a shows the CT admixtures, $|\langle +-|\Psi_{loc}^-\rangle|^2$ and $|\langle -+|\Psi_{loc}^-\rangle|^2$, as a function of $E_{CT} - E_{S_1}$ for the three values of J_C after application of the solvent-induced energy fluctuation, H', in eq 10. $|\Psi_{loc}^-\rangle$ is now defined as the lower of the two fluctuation-split levels in the upper-band. Unlike in Figure 6, the

https://doi.org/10.1021/acs.jpcc.3c06785
J. Phys. Chem. C 2024, 128, 248−260

charge asymmetry η_{CT} increases with both $E_{CT} - E_{S_1}$ and J_C. However, this coincides with a significant drop in the FE population,

$$1 - |\langle +-|\Psi^{-}_{loc}\rangle|^2 - |\langle -+|\Psi^{-}_{loc}\rangle|^2$$

and therefore oscillator strength. Our calculations show that at the null point the fraction of the oscillator strength in the upper-band decreases from about 50% for $J_C = 0.04$ eV to 27% for $J_C = 0.08$ eV. In the limit of large J_C the oscillator strength in the upper-band vanishes entirely.

Based on the above considerations, more efficient upper-band SB-CS appears to require E_{CT} to be nearly resonant with E_{S1}. However, we also need to evaluate the energetic separation between the two bands, which is important in determining whether a single laser pulse can simultaneously excite the bright, lower-band exciton as well as the degenerate upper-band states. It is also important for gauging the competition between SB-CS and interband relaxation. In order to better appreciate the energy separation, we consider the resonant case $E_{CT} - E_{S_1}$ of Figure 8a in greater detail. Use of eq 9 and eq 11 results in the *exact* values for upper-band band energy,

$$E_{k=0,+} = E_{k=\pi,+} = E_{S1} + \sqrt{t_e^2 + t_h^2} \tag{23a}$$

as well as the split H-like levels in the lower-band,

$$E_{k=\pi,-} = E_{S1} - \sqrt{t_e^2 + t_h^2} - J_C \tag{23b}$$

$$E_{k=0,-} = E_{S1} - \sqrt{t_e^2 + t_h^2} + J_C \tag{23c}$$

where from eq 11, $J_C = |2t_e t_h|/\sqrt{t_e^2 + t_h^2} \approx 2|t_h|$. (The approximate form follows when $|t_e| \gg |t_h|$.) The energetic separation between the degenerate upper band and the bright $k = 0$ state in the lower band is therefor $2\sqrt{t_e^2 + t_h^2} - J_C \approx 2|t_e| - J_C$, which is 0.16 eV in Figure 8a. We showed that the gap is further reduced to 0.06 eV with no loss in charge asymmetry when the dominant CT integral, t_e, is reduced to 0.05 eV, making it easier for a single laser pulse to simultaneously excite both bands.

As in the lower-band, the charge asymmetry can be substantially enhanced for $|E_{CT} - E_{S_1}|$ values *surrounding* the null point as J_C and t_h are both reduced while maintaining their ratio. Figure 9b shows the effect of decreasing J_C (and t_h) while maintaining the resonant condition, $J_C = 2|t_h|$ (with $t_e = 0.1$ eV throughout). As in Figure 7a, η_{CT} increases over a broader range of detunings, $E_{CT} - E_{S_1}$, as J_C diminishes, due to the enhanced insensitivity of $|E_{k=0,+} - E_{k=\pi,+}|$ to $E_{CT} - E_{S_1}$, similar to the effect in Figure 7b. Hence, both lower- and *and* upper-level SB-CS are strongly favored by smaller Coulomb couplings. Of course, the smaller J_C values will also decrease the splitting of the lower band, lowering the H-character of the absorption spectrum.

Based on Figures 8 and 9 we conclude that the most efficient upper-band SB-CS likely occurs near resonance, with $E_{CT} \approx E_{S_1}$, when $|t_e|$ dominates over both J_C and $|t_h|$. The near resonant condition is consistent with the conclusions reached in ref.[20] for the gPBI-cp complex in Figure 1, where SB-CS was attributed to the enhanced stability of the CT state (so that E_{CT} is near E_{S1}) due to the strong electron-donating ability of pyrrolidinyl substituents.

IV. DISCUSSION/CONCLUSION

Using a Hamiltonian accounting for the interaction between Frenkel and CT excitons in a molecular dimer, we investigated the impact of null points on SB-CS and NA formation. Generally, null points are defined as degeneracies within the lower or upper energy bands (i.e, "flat" bands). They occur when the set of four energy parameters, $\{J_C, t_e, t_h, E_{CT} - E_{S_1}\}$ satisfy eq 11, with the important phase relationships, $J_C t_e t_h > 0$ ($J_C t_e t_h < 0$) for lower (upper)-band null points. A class of null points with lopsided values of t_e and t_h ($|t_e| \gg |t_h|$, $|J_C|$ or $|t_h| \gg |t_e|$, $|J_C|$) were shown to be conducive to SB-CS. In this limit, null points are defined with only three parameters; $E_{CT} - E_{S_1}$, t_e, and J_C/t_h, assuming t_e is dominant. Molecular dimers with geometries consistent with such null points are extremely sensitive to solvent polarization-induced fluctuations in the electric field, which cause the degenerate adiabatic $k = 0$ and $k = \pi$ (FE/CTE) excitons to readily mix to form localized charge asymmetric states. Although the solvent perturbations are small, at a null point the response is first order in the fluctuation energy, δE, leading to a cascade effect whereby the small molecular dipole moment induced by the initial fluctuation generates a reaction field which furthers the solvent reorganization, which, in turn, increases the electric field on the dimer and so on.[5,9] Eventually, the solvent completely reorganizes around the localized charge-separated dimer (either $+-$ or $-+$) with a significant reduction in energy. The charge separation process has been treated via Marcus theory,[5,52] where ΔG_{CS} must be sufficiently negative, despite the positive value of $-T\Delta S$ from the solvent reorganization. A more detailed analysis than the present one, would treat the solvent alignment as a harmonic coordinate coupled to the induced chromophore's (or aggregate's) dipole moment.[8]

We analyzed null points in PDI dimers, showing that lower-band null points leading to efficient SB-CS (with $|t_e| \gg |t_h|$ or $|t_h| \gg |t_e|$) arise when the Coulomb coupling is relatively weak, with $|J_C|$ less than about twice the magnitude of the minor CT integral. For physically realistic PDI parameters, SB-CS is expected to be efficient for $|J_C| \lesssim 0.04$ eV, consistent with $|E_{CT} - E_{S_1}|$ less than approximately 0.1 eV, see Figures 5 and 6. The most robust SB-CS occurs when the charge asymmetry is most sensitive to polarization fluctuations, as occurs at lower-band null points when the magnitudes of J_C and the minor CT integral, e.g., t_h, become small and comparable to the fluctuation energy δE. The induced charge asymmetry becomes significant for a broad range of $E_{CT} - E_{S_1}$ values surrounding the null-point, as demonstrated in Figure 7a. In the limit $J_C = t_h = 0$, exact null points exist simultaneously in the lower and upper bands, i.e., a dual-band null point (see Figure 3c), where SB-CS can occur from either band, *independent* of $E_{CT} - E_{S_1}$. This limit may be relevant in the recent work of Sebastian and Hariharan,[17] who demonstrated efficient SB-CS in Greek-Cross PDI dimers, where the two PDIs are covalently linked in an edge-to-edge configuration with a relative twist angle of 90 deg. In ref 17, J_C and t_e, were calculated to be extremely small ($J_C \approx 4 \times 10^{-4}$ eV, $t_e \approx -0.001$ eV), while the calculated t_h is approximately 150 times larger than t_e ($t_h \approx -0.15$ eV). Efficient SB-CS was observed in polar solvents, such as acetonitrile, consistent with the theoretical predictions presented here.

Lower-band null points cannot account for the rather surprising observation of SB-CS in cofacial perylene[16,23] and PDI dimers.[19,20,24] In all such cases, the absorption spectrum

https://doi.org/10.1021/acs.jpcc.3c06785
J. Phys. Chem. C 2024, 128, 248−260

reveals H-aggregate behavior, as evidenced by a pronounced attenuation of the 0−0/0−1 vibronic peak ratio in the dimer complex compared to that in the monomer. Hence, there can be no null point in the lower-band, at least not in the ground state geometry. One possible explanation for SB-CS is the occurrence of a null point in the *upper-band*, which coexists with the H-like splitting in the lower-band, see Figure 8. However, SB-CS launched from upper-band null points has to compete with rapid interband relaxation. In addition, the higher energy of the upper-band minimizes the FE component, which reduces the absorption cross-section. Both of these detriments can be mitigated in a near-resonant upper-band null point ($E_{CT} \approx E_{S_1}$) which occurs for sufficiently stabilized (diabatic) CT states. In such cases, the degenerate upper band has a Frenkel admixture near 50% with an energy that can be only slightly greater than the bright state in the lower band (see discussion surrounding eq 23). Our hypothesis is consistent with the conclusion of ref 20, which attributes SB-CS in the gPDI-cp dimer to the enhanced stability of the CT state arising from the strong electron-donating ability of the pyrrolidinyl substituents. Moreover, a degenerate upper-level state with a roughly 50−50 admixture of FE and CT states resembles the so-called "CT-enhanced resonance states" of ref 20. As observed by Hong et al.,[20] such states eventually succumb to solvent-induced adiabatic collapse to the asymmetric charge-separated states. Similar to lower-band SB-CS, the most robust SB-CS occurs as J_C and the minor CT integral become comparable to the fluctuation energy δE, see Figure 9b. The model may account for the observations of Coleman et al.[24] who measured SB-CS in cofacial cyclophane PDI dimers with large intermolecular separations approaching 1 nm and with weak but significant H-aggregate signatures in the absorption spectrum.

In contrast to SB-CS, NA formation takes place only in the lower FE-dominated band when the diabatic FE and CTE bands are well-separated, such that $|t_e|, |t_h|, |J_C| \ll E_{CT} - E_{S_1}$. This affords a perturbative analysis, which treats the CT states as intermediate, virtual states in an effective short-range exciton coupling, J_{CT} which cancels out the Coulomb coupling, J_C[35−39] thereby making the absorption spectral line shape quite similar to that of a monomer, as experimentally verified in PDI foldamers.[40] Although NA's with lopsided $|t_e|$ and $|t_h|$ can trigger SB-CS, the initial asymmetry response to a solvent fluctuation is small due to the minor CT admixture in the degenerate adiabatic states defining the null point. Interestingly, the absorption spectrum of the SB-CS-inducing Greek-Cross dimer of Sebastian and Hariharan[17] is only slightly different from the PDI monomer spectrum, which was interpreted as evidence for NA formation. NAs were also thought to be involved in the SB-CS of covalent slip-stacked PDI dimer and trimer complexes.[26] In order to more thoroughly establish links between SB-CS and NA formation, we need to expand our analysis of SB-CS to include local vibronic coupling to the high-energy (0.15−0.18 eV) vinyl-stretching mode, which manifests as pronounced vibronic progressions in the absorption and emission spectra of PDI chromophores. In this way, we can identify signatures of SB-CS in comparison with NA formation. It may also be that vibronic coupling itself can provide the symmetry-breaking instead of solvent polarization fluctuations.[8] We also plan to include nonlocal coupling to an intermolecular "slow" mode, necessary to account for the competition between excimer formation and SB-CS.[15,16,20,21,28] It may be that a null point does not exist in the ground state geometry but is encountered during nuclear relaxation along an intermolecular coordinate subsequent to optical excitation. We plan to study such effects using the Holstein−Peierls Hamiltonian in ref 53 to account for local and nonlocal coupling. Finally, it would also be interesting to go beyond the dimer[26] to explore SB-CS in trimers and larger π-stacks which allow greater charge separation.

AUTHOR INFORMATION

Corresponding Author

Frank C. Spano − *Department of Chemistry, Temple University, Philadelphia, Pennsylvania 19122, United States;* orcid.org/0000-0003-3044-6727; Email: spano@temple.edu

Complete contact information is available at: https://pubs.acs.org/10.1021/acs.jpcc.3c06785

Notes

The author declares no competing financial interest.

ACKNOWLEDGMENTS

This work was performed under the financial support for F.C.S. from the National Science Foundation (DMR-2221923).

REFERENCES

(1) Laible, P. D.; Hanson, D. K.; Buhrmaster, J. C.; Tira, G. A.; Faries, K. M.; Holten, D.; Kirmaier, C. Switching Sides—Reengineered Primary Charge Separation in the Bacterial Photosynthetic Reaction Center. *Proc. Natl. Acad. Sci. U. S. A.* **2020**, *117*, 865−871.

(2) Cherepanov, D. A.; Shelaev, I. V.; Gostev, F. E.; Petrova, A.; Aybush, A. V.; Nadtochenko, V. A.; Xu, W.; Golbeck, J. H.; Semenov, A. Y. Primary Charge Separation within the Structurally Symmetric Tetrameric Chl2apapbchl2b Chlorophyll Exciplex in Photosystem I. *Journal of Photochemistry and Photobiology B: Biology* **2021**, *217*, No. 112154.

(3) Savikhin, S.; Jankowiak, R.: Mechanism of Primary Charge Separation in Photosynthetic Reaction Centers. In *The Biophysics of Photosynthesis*; Golbeck, J., van der Est, A., Eds.; Springer New York: New York, NY, 2014; pp 193−240.

(4) Sebastian, E.; Hariharan, M. Symmetry-Breaking Charge Separation in Molecular Constructs for Efficient Light Energy Conversion. *ACS Energy Lett.* **2022**, *7*, 696−711.

(5) Vauthey, E. Photoinduced Symmetry-Breaking Charge Separation. *ChemPhysChem* **2012**, *13*, 2001−2011.

(6) Bialas, D.; Kirchner, E.; Röhr, M. I. S.; Würthner, F. Perspectives in Dye Chemistry: A Rational Approach toward Functional Materials by Understanding the Aggregate State. *J. Am. Chem. Soc.* **2021**, *143*, 4500−4518.

(7) Young, R. M.; Wasielewski, M. R. Mixed Electronic States in Molecular Dimers: Connecting Singlet Fission, Excimer Formation, and Symmetry-Breaking Charge Transfer. *Acc. Chem. Res.* **2020**, *53*, 1957−1968.

(8) Terenziani, F.; Painelli, A.; Katan, C.; Charlot, M.; Blanchard-Desce, M. Charge Instability in Quadrupolar Chromophores: Symmetry Breaking and Solvatochromism. *J. Am. Chem. Soc.* **2006**, *128*, 15742−15755.

(9) Dereka, B.; Koch, M.; Vauthey, E. Looking at Photoinduced Charge Transfer Processes in the Ir: Answers to Several Long-Standing Questions. *Acc. Chem. Res.* **2017**, *50*, 426−434.

(10) Dereka, B.; Rosspeintner, A.; Li, Z.; Liska, R.; Vauthey, E. Direct Visualization of Excited-State Symmetry Breaking Using Ultrafast Time-Resolved Infrared Spectroscopy. *J. Am. Chem. Soc.* **2016**, *138*, 4643−4649.

(11) Dereka, B.; Svechkarev, D.; Rosspeintner, A.; Aster, A.; Lunzer, M.; Liska, R.; Mohs, A. M.; Vauthey, E. Solvent Tuning of Photochemistry Upon Excited-State Symmetry Breaking. *Nat. Commun.* **2020**, *11*, 1925.

(12) Swathi, K.; Sujith, M.; Divya, P. S.; P, M. V.; Delledonne, A.; Phan Huu, D. K. A.; Di Maiolo, F.; Terenziani, F.; Lapini, A.; Painelli, A.; et al. From Symmetry Breaking to Symmetry Swapping: Is Kasha's Rule Violated in Multibranched Phenyleneethynylenes? *Chemical Science* **2023**, *14*, 1986−1996.
(13) Terenziani, F.; Sissa, C.; Painelli, A. Symmetry Breaking in Octupolar Chromophores: Solvatochromism and Electroabsorption. *J. Phys. Chem. B* **2008**, *112*, 5079−5087.
(14) Markovic, V.; Villamaina, D.; Barabanov, I.; Lawson Daku, L. M.; Vauthey, E. Photoinduced Symmetry-Breaking Charge Separation: The Direction of the Charge Transfer. *Angew. Chem., Int. Ed.* **2011**, *50*, 7596−7598.
(15) Aster, A.; Licari, G.; Zinna, F.; Brun, E.; Kumpulainen, T.; Tajkhorshid, E.; Lacour, J.; Vauthey, E. Tuning Symmetry Breaking Charge Separation in Perylene Bichromophores by Conformational Control. *Chemical Science* **2019**, *10*, 10629−10639.
(16) Cook, R. E.; Phelan, B. T.; Kamire, R. J.; Majewski, M. B.; Young, R. M.; Wasielewski, M. R. Excimer Formation and Symmetry-Breaking Charge Transfer in Cofacial Perylene Dimers. *J. Phys. Chem. A* **2017**, *121*, 1607−1615.
(17) Sebastian, E.; Hariharan, M. Null Exciton-Coupled Chromophoric Dimer Exhibits Symmetry-Breaking Charge Separation. *J. Am. Chem. Soc.* **2021**, *143*, 13769−13781.
(18) Alzola, J. M.; Tcyrulnikov, N. A.; Brown, P. J.; Marks, T. J.; Wasielewski, M. R.; Young, R. M. Symmetry-Breaking Charge Separation in Phenylene-Bridged Perylenediimide Dimers. *J. Phys. Chem. A* **2021**, *125*, 7633−7643.
(19) Giaimo, J. M.; Gusev, A. V.; Wasielewski, M. R. Excited-State Symmetry Breaking in Cofacial and Linear Dimers of a Green Perylenediimide Chlorophyll Analogue Leading to Ultrafast Charge Separation. *J. Am. Chem. Soc.* **2002**, *124*, 8530−8531.
(20) Hong, Y.; Schlosser, F.; Kim, W.; Würthner, F.; Kim, D. Ultrafast Symmetry-Breaking Charge Separation in a Perylene Bisimide Dimer Enabled by Vibronic Coupling and Breakdown of Adiabaticity. *J. Am. Chem. Soc.* **2022**, *144*, 15539−15548.
(21) Sung, J.; Nowak-Król, A.; Schlosser, F.; Fimmel, B.; Kim, W.; Kim, D.; Würthner, F. Direct Observation of Excimer-Mediated Intramolecular Electron Transfer in a Cofacially-Stacked Perylene Bisimide Pair. *J. Am. Chem. Soc.* **2016**, *138*, 9029−9032.
(22) Kong, J.; Zhang, W.; Li, G.; Huo, D.; Guo, Y.; Niu, X.; Wan, Y.; Tang, B.; Xia, A. Excited-State Symmetry-Breaking Charge Separation Dynamics in Multibranched Perylene Diimide Molecules. *J. Phys. Chem. Lett.* **2020**, *11*, 10329−10339.
(23) Duncan, K. M.; Kellis, D. L.; Huff, J. S.; Barclay, M. S.; Lee, J.; Turner, D. B.; Davis, P. H.; Yurke, B.; Knowlton, W. B.; Pensack, R. D. Symmetry Breaking Charge Transfer in DNA-Templated Perylene Dimer Aggregates. *Molecules* **2022**, *27*, 6612.
(24) Coleman, A. F.; Chen, M.; Zhou, J.; Shin, J. Y.; Wu, Y.; Young, R. M.; Wasielewski, M. R. Reversible Symmetry-Breaking Charge Separation in a Series of Perylenediimide Cyclophanes. *J. Phys. Chem. C* **2020**, *124*, 10408−10419.
(25) Wu, Y.; Young, R. M.; Frasconi, M.; Schneebeli, S. T.; Spenst, P.; Gardner, D. M.; Brown, K. E.; Würthner, F.; Stoddart, J. F.; Wasielewski, M. R. Ultrafast Photoinduced Symmetry-Breaking Charge Separation and Electron Sharing in Perylenediimide Molecular Triangles. *J. Am. Chem. Soc.* **2015**, *137*, 13236−13239.
(26) Lin, C.; Kim, T.; Schultz, J. D.; Young, R. M.; Wasielewski, M. R. Accelerating Symmetry-Breaking Charge Separation in a Perylenediimide Trimer through a Vibronically Coherent Dimer Intermediate. *Nat. Chem.* **2022**, *14*, 786−793.
(27) Wang, K.; Shao, G.; Peng, S.; You, X.; Chen, X.; Xu, J.; Huang, H.; Wang, H.; Wu, D.; Xia, J. Achieving Symmetry-Breaking Charge Separation in Perylenediimide Trimers: The Effect of Bridge Resonance. *J. Phys. Chem. B* **2022**, *126*, 3758−3767.
(28) Sebastian, E.; Sunny, J.; Hariharan, M. Excimer Evolution Hampers Symmetry-Broken Charge-Separated States. *Chemical Science* **2022**, *13*, 10824−10835.
(29) Hong, Y.; Kim, W.; Kim, T.; Kaufmann, C.; Kim, H.; Würthner, F.; Kim, D. Real-Time Observation of Structural Dynamics Triggering Excimer Formation in a Perylene Bisimide Folda-Dimer by Ultrafast Time-Domain Raman Spectroscopy. *Angew. Chem., Int. Ed.* **2022**, *61*, No. e202114474.
(30) Giaimo, J. M.; Lockard, J. V.; Sinks, L. E.; Scott, A. M.; Wilson, T. M.; Wasielewski, M. R. Excited Singlet States of Covalently Bound, Cofacial Dimers and Trimers of Perylene-3,4:9,10-Bis-(Dicarboximide)S. *J. Phys. Chem. A* **2008**, *112*, 2322−2330.
(31) Son, M.; Park, K. H.; Shao, C.; Würthner, F.; Kim, D. Spectroscopic Demonstration of Exciton Dynamics and Excimer Formation in a Sterically Controlled Perylene Bisimide Dimer Aggregate. *J. Phys. Chem. Lett.* **2014**, *5*, 3601−3607.
(32) Bae, Y. J.; Shimizu, D.; Schultz, J. D.; Kang, G.; Zhou, J.; Schatz, G. C.; Osuka, A.; Wasielewski, M. R. Balancing Charge Transfer and Frenkel Exciton Coupling Leads to Excimer Formation in Molecular Dimers: Implications for Singlet Fission. *J. Phys. Chem. A* **2020**, *124*, 8478−8487.
(33) Margulies, E. A.; Shoer, L. E.; Eaton, S. W.; Wasielewski, M. R. Excimer Formation in Cofacial and Slip-Stacked Perylene-3,4:9,10-Bis(Dicarboximide) Dimers on a Redox-Inactive Triptycene Scaffold. *Phys. Chem. Chem. Phys.* **2014**, *16*, 23735−23742.
(34) Mauck, C. M.; Young, R. M.; Wasielewski, M. R. Characterization of Excimer Relaxation Via Femtosecond Shortwave- and Mid-Infrared Spectroscopy. *J. Phys. Chem. A* **2017**, *121*, 784−792.
(35) Hestand, N. J.; Spano, F. C. Expanded Theory of H- and J-Molecular Aggregates: The Effects of Vibronic Coupling and Intermolecular Charge Transfer. *Chem. Rev.* **2018**, *118*, 7069−7163.
(36) Hestand, N. J.; Spano, F. C. Molecular Aggregate Photophysics Beyond the Kasha Model: Novel Design Principles for Organic Materials. *Acc. Chem. Res.* **2017**, *50*, 341−350.
(37) Hestand, N. J.; Spano, F. C. Interference between Coulombic and Ct-Mediated Couplings in Molecular Aggregates: H- to J-Aggregate Transformation in Perylene-Based Pi-Stacks. *J. Chem. Phys.* **2015**, *143*, No. 244707.
(38) Yamagata, H.; Maxwell, D. S.; Fan, J.; Kittilstved, K. R.; Briseno, A. L.; Barnes, M. D.; Spano, F. C. Hj-Aggregate Behavior of Crystalline 7,8,15,16-Tetraazaterrylene: Introducing a New Design Paradigm for Organic Materials. *J. Phys. Chem. C* **2014**, *118*, 28842−28854.
(39) Yamagata, H.; Pochas, C. M.; Spano, F. C. Designing J- and H-Aggregates through Wave Function Overlap Engineering: Applications to Poly(3-Hexylthiophene). *J. Phys. Chem. B* **2012**, *116*, 14494−14503.
(40) Kaufmann, C.; Bialas, D.; Stolte, M.; Würthner, F. Discrete Π-Stacks of Perylene Bisimide Dyes within Folda-Dimers: Insight into Long- and Short-Range Exciton Coupling. *J. Am. Chem. Soc.* **2018**, *140*, 9986−9995.
(41) Nayak, N.; Gopidas, K. R. Self-Assembly of a B-Cyclodextrin Bis-Inclusion Complex into a Highly Crystalline Fiber Network. An Effective Strategy for Null Aggregate Design. *J. Phys. Chem. B* **2019**, *123*, 8131−8139.
(42) Lijina, M. P.; Benny, A.; Ramakrishnan, R.; Nair, N. G.; Hariharan, M. Exciton Isolation in Cross-Pentacene Architecture. *J. Am. Chem. Soc.* **2020**, *142*, 17393−17402.
(43) Lijina, M. P.; Benny, A.; Sebastian, E.; Hariharan, M. Keeping the Chromophores Crossed: Evidence for Null Exciton Splitting. *Chem. Soc. Rev.* **2023**, *52*, 6664−6679.
(44) Bo, Y.; Hou, P.; Wan, J.; Cao, H.; Liu, Y.; Xie, L.; Guldi, D. M. One-Pot Synthesis and Excited-State Dynamics of Null Exciton-Coupled Diketopyrrolopyrroles Oligo-Grids. *Adv. Mater.* **2023**, *35*, No. 2302664.
(45) Oleson, A.; Zhu, T.; Dunn, I. S.; Bialas, D.; Bai, Y.; Zhang, W.; Dai, M.; Reichman, D. R.; Tempelaar, R.; Huang, L. B.; et al. Perylene Diimide-Based Hj- and Hj-Aggregates: The Prospect of Exciton Band Shape Engineering in Organic Materials. *J. Phys. Chem. C* **2019**, *123*, 20567−20578.
(46) Weller, A. Photoinduced Electron Transfer in Solution: Exciplex and Radical Ion Pair Formation Free Enthalpies and Their Solvent Dependence. *Zeitschrift für Physikalische Chemie* **1982**, *133*, 93−98.
(47) Gisslen, L.; Scholz, R. Crystallochromy of Perylene Pigments: Interference between Frenkel Excitons and Charge-Transfer States. *Phys. Rev. B* **2009**, *80*, No. 115309.

https://doi.org/10.1021/acs.jpcc.3c06785
J. Phys. Chem. C 2024, 128, 248−260

(48) Merrifield, R. E. Ionized States in a One-Dimensional Molecular Crystal. *J. Chem. Phys.* **1961**, *34*, 1835−1839.
(49) Strong, S. E.; Hestand, N. J. Modeling Nonlocal Electron−Phonon Coupling in Organic Crystals Using Interpolative Maps: The Spectroscopy of Crystalline Pentacene and 7,8,15,16-Tetraazaterrylene. *J. Chem. Phys.* **2020**, *153*, No. 124113.
(50) Hestand, N. J.; Tempelaar, R.; Knoester, J.; Jansen, T. L. C.; Spano, F. C. Exciton Mobility Control through Sub-Angstrom Packing Modifications in Molecular Crystals. *Phys. Rev. B* **2015**, *91*, No. 195315.
(51) Gisslen, L.; Scholz, R. Crystallochromy of Perylene Pigments: Influence of an Enlarged Polyaromatic Core Region. *Phys. Rev. B* **2011**, *83*, No. 155311.
(52) Sebastian, E.; Hariharan, M. A Symmetry-Broken Charge-Separated State in the Marcus Inverted Region. *Angew. Chem., Int. Ed.* **2023**, *62*, No. e202216482.
(53) Bialas, A. L.; Spano, F. C. A Holstein−Peierls Approach to Excimer Spectra: The Evolution from Vibronically Structured to Unstructured Emission. *J. Phys. Chem. C* **2022**, *126*, 4067−4081.

https://doi.org/10.1021/acs.jpcc.3c06785
J. Phys. Chem. C 2024, 128, 248−260